

The Puzzling Superorbital Period Variation of the Low-mass X-ray Binary 4U 1820-30

YI CHOU (周翊),¹ JUN-LEI WU (吳君磊),¹ BO-CHUN CHEN (陳泊鎔),¹ AND WEI-YUN CHANG (張瑋芸)¹

¹*Graduate Institute of Astronomy, National Central University
300 Zhongda Rd. Zhongli Dist. Taoyuan, 320317, Taiwan*

ABSTRACT

Because of the previously observed stability of the 171-day period, the superorbital modulation of the low-mass X-ray binary 4U 1820-30 was considered a consequence of a third star orbiting around the binary. This study aims to further verify this triple model by testing the stability of superorbital period using the light curves collected by X-ray sky monitoring/scanning telescopes from 1987 to 2023. Both power spectral and phase analysis results indicate a significant change in the superorbital period from 171 days to 167 days over this 36-year span. The evolution of the superorbital phase suggests that the superorbital period may have experienced an abrupt change between early 2001 and mid-2003 or changed gradually with a period derivative of $\dot{P}_{sup} = (-4.20 \pm 0.72) \times 10^{-4}$ day/day. We conclude that the superorbital period of 4U 1820-30 was not as stable as anticipated by the triple model, which strongly challenges this hypothesis. Instead, we propose an irradiation-induced mass transfer instability scenario to explain the superorbital modulation of 4U 1820-30.

1. INTRODUCTION

4U 1820-30, discovered by [Giacconi et al. \(1974\)](#), is an ultra-compact low mass X-ray binary (LMXB) located near the center of globular cluster NGC 6624. It was the first X-ray source known to exhibit Type-I X-ray burst ([Grindlay et al. 1976](#)), indicating that the accretor in this binary system is a neutron star. Its 685 s orbital period, discovered by [Stella et al. \(1987\)](#) from its sinusoidal-like orbital modulation in the X-ray light curve, makes 4U 1820-30 the most compact LMXB. The mass-losing companion is a Roche-lobe filling helium white dwarf with a mass of 0.06-0.08 M_{\odot} ([Rappaport et al. 1987](#)). Mass transfer in the system is induced by the orbital angular momentum loss through gravitational radiation, which should result in a positive orbital period derivative with a lower limit of $\dot{P}_{orb}/P_{orb} > 8.8 \times 10^{-8} yr^{-1}$ ([Rappaport et al. 1987](#)). However, observed orbital period derivatives reported by [Tan et al. \(1991\)](#); [van der Klis et al. \(1993a,b\)](#), [Chou & Grindlay \(2001\)](#) (hereafter CG01), and [Peuten et al. \(2014\)](#) were negative with the latest value of $\dot{P}_{orb}/P_{orb} = (-5.21 \pm 0.13) \times 10^{-8} yr^{-1}$ updated by [Chou & Jhang \(2023\)](#), evaluated from ~ 46 years of orbital phase evolu-

tion. This contradiction is believed due to the binary system accelerating by the gravitational potential in NGC 6624 ([Tan et al. 1991](#); [Chou & Grindlay 2001](#); [Peuten et al. 2014](#); [Chou & Jhang 2023](#)). Additionally, superhump modulation with a period of 691.6 ± 0.7 s, $\sim 1\%$ significantly longer than the orbital period, was observed in both FUV ([Wang & Chakrabarty 2010](#)) and X-ray ([Chou & Jhang 2023](#)) bands. From the superhump period, the mass of companion of 4U 1820-30 was estimated as $0.07M_{\odot}$ ([Wang & Chakrabarty 2010](#); [Chou & Jhang 2023](#)).

In addition to orbital and superhump variations, 4U 1820-30 exhibits superorbital modulation with a period much longer than its orbital period. [Priedhorsky & Terrell \(1984\)](#) discovered the X-ray flux modulation by a factor of 2 with a period of 176.4 ± 1.3 days using the light curve detected by Vela 5B from 1969 to 1976. This periodicity was further confirmed by [Smale & Lochner \(1992\)](#). However, by analyzing the light curve collected between 1996 and 2000 by All Sky Monitor on-board Rossi X-ray Timing Explorer (RXTE ASM), CG01 revised the superorbital period to 171.39 ± 1.93 days. Combining the times of the flux minima of the superorbital modulation (hereafter superorbital minima) detected by Vela 5B and All Sky Monitor onboard Ginga (Ginga ASM), CG01 further constrained the period to be 171.033 ± 0.326 days and claimed that the superorbital period was stable over ~ 30 years with $|\dot{P}_{sup}/P_{sup}| < 2.2 \times 10^{-4} yr^{-1}$. Based on the stabil-

ity of the superorbital period, CG01 proposed that this long-term variability is due to a hierarchical third star orbiting around the binary system (Grindlay 1986, 1988, hereafter the triple model). The hierarchical third component can cause the eccentricity of inner binary system to vary with a period (P_{ecc}) as

$$P_{ecc} = K \frac{P_3^2}{P_{orb}} \quad (1)$$

where P_3 is the orbital period of third star, P_{orb} is the binary orbital period and K is a constant of unity (Mazeh & Shaham 1979). Because the mass transfer rate is highly sensitive to the Roche lobe radius, which is proportional to the binary separation, the variation of binary eccentricity can cause the mass loss rate and the accretion rate to change with a period of P_{ecc} and thus $P_{sup} = P_{ecc}$. For the 4U 1820-30 system, the orbital period of the third companion is estimated to be ~ 1.1 days for $K \sim 1$, and beat sidebands resulting from coupling binary modulation and ~ 1.1 day periodicity may be observable in the power spectrum. Although these beat sidebands were not detected in RXTE observations (CG01), Chou & Jhang (2023) suggested that the 691.6 ± 0.7 s periodicity observed in the X-ray band might be caused by a hierarchical triple orbiting around the binary system with an orbital period of 0.8 days. Moreover, CG01 found that the active times of Type-I X-ray bursts were clustered within ± 23 days of expected superorbital minima, which aligns with the observation that the bursts can be seen only in low state (Clark et al. 1977; Stella et al. 1984). This fact implies that the superorbital modulation of 4U 1820-30 is due to changes in the accretion rate rather than external occultation or absorption effects, which is consistent with the triple model.

The periodicity of 171 days was further confirmed by Šimon (2003); Wen et al. (2006); Zdziarski et al. (2007a); Kotze & Charles (2012) using additional RXTE ASM data and by Farrell et al. (2009) using the data collected by Burst Alert Telescope onboard the Neil Gehrels Swift Observatory (Swift BAT). Applying the triple model, Zdziarski et al. (2007a) demonstrated that the factor of 2 superorbital modulation in X-ray light curve can be explained by the eccentricity of inner binary oscillating between 0 and 0.004. The discovery of the dependence of orbital modulation profile on the accretion rate (Zdziarski et al. 2007b) also supports the triple model. The hard X-ray light curve collected from Swift BAT showed that the superorbital modulation can be observable only for the energy bands less than 24 keV (Farrell et al. 2009). Conversely, by comparing the peak widths of the power spectra made from light

curves detected by RXTE ASM and Swift BAT with the corresponding simulated light curves, Farrell et al. (2009) found that the peak widths from real data are marginally wider than the ones from simulated data, concluding that this may be caused by the superorbital period change. Kotze & Charles (2012) adopted the dynamic power spectrum technique to analyze the superorbital variability of several X-ray binaries, and found no significant superorbital period change for 4U 1820-30 except for a weakening of power during MJD $\sim 51,200$ -52,200.

Owing to the monitoring/scanning X-ray telescopes, 4U 1820-30 has been observed for decades and is still being monitored by the Swift BAT the Monitor of All-sky X-ray Image (MAXI), and Fermi Gamma-ray Burst Monitor (Fermi GBM). In this work, we aim to further verify the stability of the superorbital period, which is the crucial evidence for the triple model of 4U 1820-30 system, and to establish an updated ephemeris for superorbital modulation. In this paper, we introduce the instruments used to obtain the light curves for this research, including Ginga ASM, RXTE ASM, Swift BAT, MAXI, and Fermi GBM as well as the light curve collected by RXTE Proportional Counter Array (RXTE PCA) while it processed the monitoring observations of the Galactic center and plane (Markwardt 2006), in Section 2. A preliminary superorbital period stability test was performed using the power spectrum made by the entire light curve of each instrument (Section 3.1). A more detailed measurement of superorbital period variation was obtained by analyzing the superorbital phase evolution and updating the ephemerides (Section 3.2). The new ephemerides allow us to verify whether the Type-I X-ray bursts occur clustered around the expected superorbital minima. In Section 4, we discuss the instability of superorbital period, which poses a serious challenge of the triple model, and explore the possible interpretations for the superorbital period variation of 4U 1820-30.

2. OBSERVATIONS

The Ginga ASM consisted of two identical gas proportional counters with six fan-beam collimators to restrict field of view (FOV) of $1^\circ \times 45^\circ$. It was sensitive to X-ray photons with energies between 1 and 20 keV, and had a total effective area of 420 cm². It provided real-time alerts of X-ray transient phenomena and long-term historical records of X-ray sources. The Ginga ASM monitored the sky from 1987 February to 1991 October. Further details of the Ginga ASM are described by Tsunemi et al. (1989). The Ginga ASM light curve of 4U 1820-30 archived on the web-

site of the High Energy Astrophysics Science Archive Research Center (HEASARC¹) collected from March 7, 1987 (MJD 46,861) to October 3, 1991 (MJD 48,532) was analyzed in this study.

The RXTE ASM (Levine et al. 1996) was an instrument mounted on RXTE to monitor the variable and the transient X-ray sources. It consisted of three scanning shadow cameras, each containing a position-sensitive proportional counter, to observe the sky through a one-dimensional coded mask with an FOV of $6^\circ \times 90^\circ$. It was designed to detect the cosmic X-rays in the photon energy range of 1.5-12 keV, which can be further divided into 1.5-3, 3-5 and 5-12 keV energy bands. In addition to these energy bands, the light curves with two different time resolutions, dwell (a 90 sec exposure) and one-day binned, were also archived. During its mission, from the beginning of 1996 to early 2012, the RXTE ASM scanned the entire sky every 90 minutes. In this research, the 1.5-12 keV RXTE ASM light curve of 4U 1820-30 archived on the website of the HEASARC collected between January 6, 1996 (MJD 50,088) and September 27, 2011 (MJD 55,831) was selected to analyze the superorbital modulation of 4U 1820-30.

In addition to the regular pointing observations, the RXTE PCA also conducted monitoring observations of the galactic center and plane starting from 1999 (Markwardt 2006). The PCA was an instrument with an effective area of 6500 cm² designed to detect the X-ray photons in the energy range of 2-60 keV (Jahoda et al. 1996). Despite being a non-imaging instrument, its 1° FOV, constrained by collimators, allowed for identification and detection of X-ray sources. It scanned over galactic bulge and plane approximately twice per week (Markwardt 2006), providing sufficient cadence to resolve the superorbital modulation of 4U 1820-30. The light curve of 4U 1820-30 collected by PCA in this program from February 5, 1999 (MJD 51,214) to October 30 2011 (MJD 55,846) was available on the program website².

The BAT, an instrument on Swift, is a coded-mask telescope with a large FOV (1.4 steradian) to monitor the hard X-ray sky in the energy range 15-150 keV since 2004 (Barthelmy et al. 2005). Apart from triggering alerts for gamma-ray bursts, its angular resolution ($\sim 20'$) and large photon collecting area (5200 cm²) enable monitoring of the known cosmic X-ray sources as the Swift satellite orbits around the Earth every ~ 96 minutes. This capability allows for the study of long-

term variability these sources. In this work, we analyzed the daily binned light curve of 4U 1820-30 that archived on the Swift website³ observed from February 14, 2005 (MJD 53,415) through August 1, 2023 (MJD 60,157).

The MAXI, installed on the Japanese Experiment Module of International Space Station (ISS), is designed to alert the transient X-ray sources and monitor the long-term variations of the X-ray sources (Matsuoka et al. 2009). It contains two types of slit cameras with two different detectors: a gas proportional counter with an effective area of 5250 cm² for detecting the X-ray photons in the energy range of 2-30 keV, and a solid state camera with an effective area of 200 cm² sensitive to the X-ray photons in the energy range of 0.5-12 keV. MAXI can scan almost the entire sky twice during each ISS orbit (~ 90 minutes). In this study, we analyzed the daily binned light curve of the energy range of 2-20 keV collected between 2009 August 12 (MJD 55,055) and 2023 August 1 (MJD 60,157), available on the MAXI on-demand process website⁴, to study the superorbital modulation of 4U 1820-30.

The Fermi GBM is an all-sky monitoring instrument onboard the Fermi Gamma-ray Space Telescope, launched in 2008 (Meegan et al. 2009). Designed to observe gamma-ray bursts and other transient phenomena using the Earth occultation technique (Wilson-Hodge et al. 2012), the GBM covers a broad energy range from 8 keV to 40 MeV. It consists of 12 sodium iodide (NaI) detectors, optimized for the low-energy range, and two bismuth germanate (BGO) detectors for higher energies, strategically placed to provide nearly full-sky coverage. The GBM enables rapid localization and characterization of transient gamma-ray events, supporting follow-up observations by other instruments and ground-based facilities. The Fermi GBM light curve of 4U 1820-30 is available on the website of Gamma-Ray Astrophysics Team, National Space, Science, and Technology Center (NSSTC)⁵. In this work, we analyzed the daily binned light curve in the energy range of 12-25 keV collected between 2012 February 9 (MJD 55966), the earliest record in the archived light curve, and 2023 August 1 (MJD 60,157).

The light curves of 4U 1820-30 collected by these six instruments are shown in Figure 1.

3. DATA ANALYSIS

¹ <https://heasarc.gsfc.nasa.gov/docs/archive.html>

² https://asd.gsfc.nasa.gov/Craig.Markwardt//galscan/html/4U_1820-30.html

³ <https://swift.gsfc.nasa.gov/results/transients/H1820-303/>

⁴ <http://maxi.riken.jp/mxondem>

⁵ https://gammaray.nsstc.nasa.gov/gbm/science/earth_occ/H1820-303.html

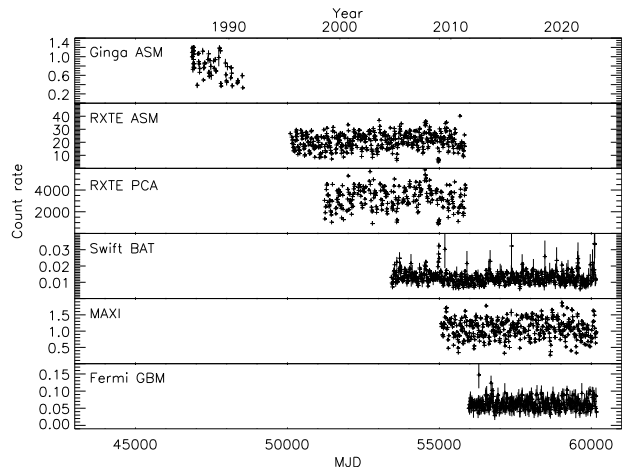


Figure 1. Light curves collected by six instruments for analysis in this work. The bin size of these light curves is 10 days.

3.1. Power Spectral Analysis

In the power spectral analysis, all the light curves were rebinned into daily averages for consistency. To probe the superorbital periods of various observations, the Lomb-Scargle (LS) periodogram (Scargle 1982) was applied to generate the power spectra. We set the frequency resolution to 2×10^{-6} cycles/day and then applied the cubic spline interpolation around the peaks of the power spectra to further refine their locations. The errors of signal frequencies were estimated by the method proposed by Horne & Baliunas (1986):

$$\delta f = \frac{3\sigma_N}{4N_0^{1/2}TA} \quad (2)$$

where A is the amplitude of the signal, σ_N^2 is the variance of the noise after the signal being removed, T is the time span of the light curve and N_0 is the number of data points. If both signals of the fundamental and second harmonics frequencies are significantly detected, the amplitudes of these components were determined by fitting a two-component sinusoidal function to the light curve, with the frequencies fixed at the signal frequencies derived from the power spectrum. Otherwise, a single sinusoidal function was fitted. σ_N^2 was estimated as the root-mean-square (rms) of the residuals after subtracting the best-fitting sinusoidal function from the light curve.

The power spectra are depicted in Figure 2. Significant superorbital signals are evident in the power spectra of all six instruments. Additionally, the second harmonic signals are detectable in the data from the more sensitive instruments, including RXTE ASM, RXTE PCA, Swift BAT, and MAXI. The detected su-

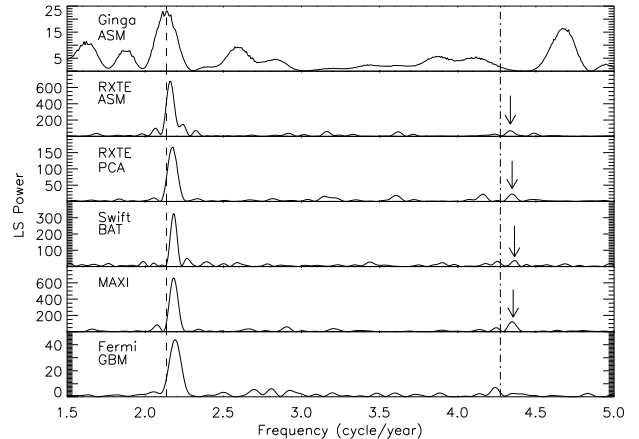


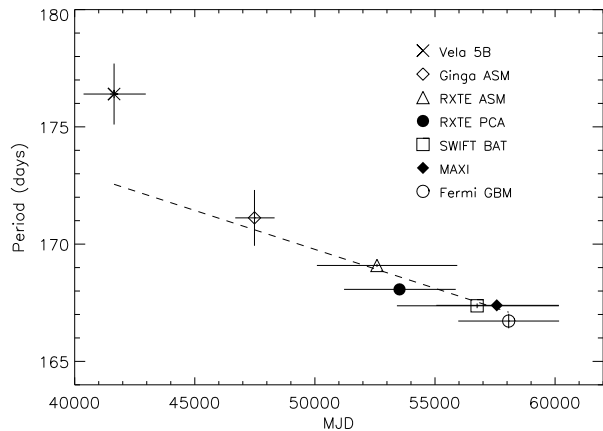
Figure 2. Power spectra derived from the light curves collected by six instruments in this work. Significant signals corresponding to the fundamental frequency of the superorbital modulations are visible, while signals of the second harmonic, indicated by arrows, are also detectable with higher-sensitivity instruments. The vertical dashed line marks the superorbital frequency from the CG01 ephemeris ($f = 2.136$ cycles/year), and the dashed-dotted line represents its second harmonic ($f = 4.272$ cycles/year). Except for the power spectrum from the Ginga ASM data, notable deviations in the superorbital frequency compared to the one proposed by CG01 can be observed in both the first and second harmonic peaks in the power spectra.

perorbital periods and their corresponding second harmonic periods are summarized in Table 1. It is apparent that the superorbital periods deviate from the period proposed by CG01, except for the one evaluated from Ginga ASM data, showing a tendency to decrease over time. By incorporating the superorbital period reported by (Priedhorsky & Terrell 1984) from the Vela 5B light curve, we estimated the timescale of the superorbital change by fitting a linear function to the detected superorbital periods over time (see Figure 3). This result in a period derivative of $\dot{P}_{sup}/P_{sup} = (-7.13 \pm 0.33) \times 10^{-4} \text{ yr}^{-1}$, corresponding to an evolution timescale of 1,403 years. This period derivative exceeds the upper limit proposed by CG10 ($|\dot{P}_{sup}/P_{sup}| < 2.2 \times 10^{-4} \text{ yr}^{-1}$). However, the linear fitting yielded a reduced χ^2 of 12.2, suggesting that the superorbital period evolution of 4U 1820-30 is likely more complex than the constant period derivative model suggests. Further variations in the superorbital period from phase analysis will be demonstrated in Section 3.2.

Additionally, to compare the amplitudes of superorbital modulation, we folded these six light curves using two kinds of linear ephemeris. The first one is the

Table 1. Superorbital Period and RMS Amplitude Measured from the Light Curves Collected by Different Instruments

Instrument	Energy Rang (keV)	Duration (MJD)	Superorbital	2nd Harmodic	RMS AMP	RMS AMP
			Period (Days)	Period (Days)	(CG01 ephemeris) (%)	(Local ephemeris) (%)
Ginga ASM	1-20	46,861-48,532	170.95±1.16	-	33	36
RXTE ASM	1.5-12	50,083-55,927	169.03±0.06	84.25±0.04	12	18
RXTE PCA	2-60	51,215-55,864	168.06±0.09	84.04±0.06	12	21
Swift BAT	15-50	53,415-60,157	167.62±0.10	83.80±0.06	7.6	15
MAXI	2-20	55,055-60,157	167.40±0.06	83.06±0.04	10	20
Fermi GBM	12-25	55,967-60,157	166.62±0.34	-	11	15

**Figure 3.** Superorbital periods measured from 6 different instruments, including the one from Vela 5B observation reported by Friedhorsky & Terrell (1984). The horizontal lines indicate the durations of the corresponding light curves, and the dashed line represents the best fit of a linear model to estimate the period change rate, which yields a period derivative of $\dot{P}/P = (-7.13 \pm 0.33) \times 10^{-4} \text{ yr}^{-1}$

optimal ephemeris proposed by CG01 (hereafter CG01 ephemeris),

$$\begin{aligned}
 T_N &= JD2,450,909.9 + 171.033 \times N \\
 &= MJD50,909.4 + 171.033 \times N
 \end{aligned}
 \quad (3)$$

The other one is the local ephemeris, with a folding period corresponding to the best period obtained by the power spectrum (see Table 1), along with an arbitrary phase zero epoch for each light curve. The rms amplitudes folded by both types of ephemeris are listed in Table 1. The rms amplitudes of the profiles folded by the corresponding local ephemerides are significantly larger than those folded by CG01 ephemeris, indicating that the CG01 ephemeris is no longer suitable. This shows that the superorbital period of 4U 1820-30 has undergone significant changes during 1987 to 2023.

3.2. Superorbital Phase Evolution

In this research, we aimed to trace the long-term evolution of the superorbital phase of 4U 1820-30, necessitating the analysis of superorbital phases measured from different instruments. However, time lags between different energy bands are often observed in astronomical time series. For instance, soft phase lags of pulsed emissions are commonly noted in accreting millisecond X-ray pulsars (Cui et al. 1998; Patruno & Watts 2021). Hence, a coherence test was conducted to verify if there was a significant time lag between any of two light curves from different instruments. However, this test could be only performed on the light curves with overlapping observation times. For each pair of light curves, only overlapping parts were selected for coherence test. The power spectra were obtained the superorbital periods for the corresponding light curves. The superorbital modulation profiles of both light curves were conducted by folding the mean period measured from the power spectra with an arbitrary but fixed phase zero epoch. We discovered that all the profiles could be well fitted with a four-component sinusoidal function, that is, $r(\phi) = a_0 + \sum_{k=1}^4 [a_k \cos(2\pi k\phi) + b_k \sin(2\pi k\phi)]$. To measure the possible time delay between the two instruments, we applied the cross-correlation between the best-fitted modulation profiles. The test results are shown in Table 2. The phase difference is generally no more than 0.026 cycle, which is much smaller the phase jitters (~ 0.1 cycle, see CG01). We conclude that no significant systematic time delay is observable among these instruments for the superorbital modulation of 4U 1820-30.

To trace the evolution of superorbital phase, we segmented the light curves and folded them to derive the modulation profiles. For instruments highly sensitive to superorbital modulation, like RXTE ASM and MAXI light curves, two cycles (2×171 days) per segment sufficed to yield clear profiles. In the case of Swift BAT observations, where no superorbital modulation

Table 2. Coherence Test for RXTE ASM, RXTE PCA, Swift BAT, MAXI and Fermi GBM Light Curves

Instrument 1	Instrument 2	Overlapping Time (MJD)	Phase lag ($\phi_1 - \phi_2$)
RXTE ASM	RXTE PCA	51,215-55,864	-0.009
RXTE ASM	Swift BAT	53,415-55,927	0.022
RXTE ASM	MAXI	55,055-55,927	-0.036
RXTE PCA	SWIFT BAT	53,415-55,864	0.022
RXTE PCA	MAXI	55,055-55,864	-0.007
Swift BAT	MAXI	55,055-60,157	-0.021
Swift BAT	Fermi GBM	55,967-60,157	-0.001
MAXI	Fermi GBM	55,967-60,157	-0.009

was detected for the photon energies higher than 24 keV (Farrell et al. 2009), we selected four cycles as a data segment to ensure significant profile detection. As for the RXTE PCA light curve, due to the observation gaps, we adopted four cycles per segment to create the profiles. However, only three data segments provided sufficient phase coverage for further analysis. Given the very low sensitivity of Ginga ASM, a clear profile could only be obtained by folding the entire light curve.

Following the approach of CG01, we selected the superorbital minimum as the fiducial point of the superorbital phase. Ideally, we would fold a light curve segment using a fixed ephemeris, such as the CG01 ephemeris (Eq. 3) to determine the phase (i.e. ϕ_{CG01}). However, as indicated in Section 3.1, the CG01 ephemeris is unlikely to be an optimal ephemeris for the all observations, particularly for recent ones (e.g. Swift BAT, MAXI, and Fermi GBM observations), which could lead to profile deformation. To precisely determine the ϕ_{CG01} , we folded the light curve segments using the optimal linear ephemeris specific to each instrument (local ephemeris). This involved folding the data on the period obtained from power spectral analysis (see Table 1) and an arbitrary but fixed phase zero epoch. A typical modulation profile is depicted in Figure 4. The phase (ϕ_{local}) of a data segment was determined by fitting a four-component sinusoidal function and identifying the phase corresponding to the intensity minimum (fiducial point). This phase value, along with the local ephemeris, facilitated the evaluation of the superorbital minimum time (t_m) closest to the mid of observation time of the data segment. Subsequently, t_m was then folded by CG01 ephemeris (Eq. 3) to obtain the phase ϕ_{CG01} .

The superorbital orbital phases (ϕ_{CG01}) are listed in Table 3, and their evolution is illustrated in Fig-

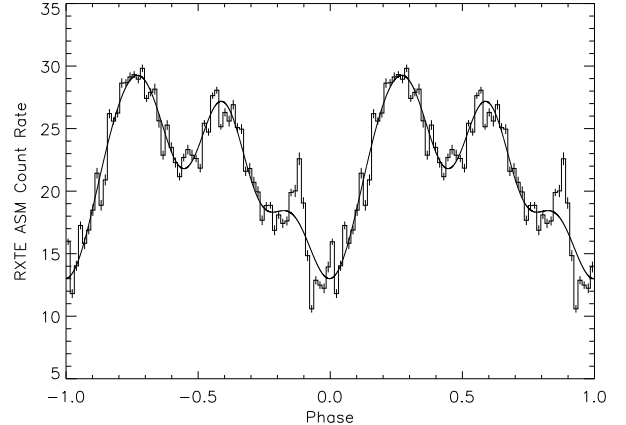


Figure 4. A typical superorbital modulation profile of a data segment created by folding the light curve collected by RXTE ASM from MJD 54,158.64 to 54,497.86 (~ 2 cycles) with a folding period of 169.09 days from power spectral analysis (Section 3.1) and an arbitrary phase zero epoch. The solid line represents the optimal fit of a 4-component sinusoidal function to locate the superorbital minimum phase ϕ_{local} . A BLS feature found by Šimon (2003) can be also observed.

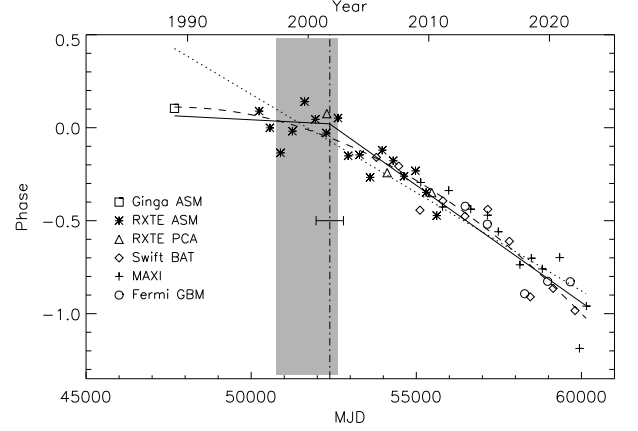
ure 5. It is noteworthy that while the superorbital modulation displays strong periodicity in the power spectra, the modulation profile varies from cycle to cycle, exhibiting the quasi-periodic nature as described in Zdziarski et al. (2007a). This variability induces phase jitters of ~ 0.1 cycle, evident in Figure 5 and CG01. These phase jitters are considerably larger than the error estimated from photon statistics (~ 0.005 cycle). Despite the presence of phase jitters, a discernible phase evolution trend can be discerned in Figure 5. However, independently evaluating errors from phase jitters is difficult, which depend on the evolution model. In the subsequent analysis, we utilized the unweighted fitting method outlined by Press et al. (2002) to update the ephemeris for the superorbital modulation of 4U 1820-30.

3.2.1. Linear Model

According to the triple model, the period should be remain stable from a long-term perspective because the superorbital modulation is induced by a hierarchical third component orbiting around the binary system. Therefore, our initial approach involved fitting a linear function to the phase evolution as depicted in Figure 5. The parameters of the optimal linear function are listed in Table 4 yielding a period of 167.99 ± 0.16 days with a phase zero epoch of $\text{MJD } 50,932.72 \pm 5.19$. We assessed

Table 3. Superorbital Phase (ϕ_{CG01}) of 4U 1820-30

Superorbital minimum Time (MJD)	Phase (ϕ_{CG01})	Instrument
47,677.560	0.1040	Ginga ASM
50,240.528	0.0892	RXTE ASM
50,567.180	-0.0009	RXTE ASM
50,886.301	-0.1351	RXTE ASM
51,248.266	-0.0187	RXTE ASM
51,617.490	0.1401	RXTE ASM
51,943.259	0.0448	RXTE ASM
52,272.795	-0.0285	RXTE ASM
52,290.171	0.0755	RXTE PCA
52,628.569	0.0517	RXTE ASM
52,935.953	-0.1511	RXTE ASM
53,278.853	-0.1462	RXTE ASM
53,600.247	-0.2671	RXTE ASM
53,789.674	-0.1595	Swift BAT
53,967.300	-0.1210	RXTE ASM
54,117.222	-0.2421	RXTE PCA
54,299.651	-0.1778	RXTE ASM
54,465.782	-0.2065	Swift BAT
54,627.524	-0.2608	RXTE ASM
54,974.529	-0.2319	RXTE ASM
55,109.387	-0.4434	Swift BAT
55,296.737	-0.3480	RXTE ASM
55,132.435	-0.2946	MAXI
55,467.179	-0.3491	RXTE PCA
55,617.470	-0.4727	RXTE ASM
55,794.143	-0.4257	MAXI
55,802.064	-0.3934	Swift BAT
55,980.165	-0.3381	MAXI
56,472.080	-0.4760	Swift BAT
56,478.810	-0.4226	Fermi GBM
56,647.187	-0.4381	MAXI
57,162.582	-0.4387	Swift BAT
57,149.732	-0.5190	Fermi GBM
57,154.762	-0.4704	MAXI
57,481.630	-0.5593	MAXI
57,817.333	-0.6105	Swift BAT
58,135.365	-0.7370	MAXI
58,279.709	-0.8931	Fermi GBM
58,450.326	-0.9095	Swift BAT
58,483.492	-0.7016	MAXI
58,815.675	-0.7594	MAXI
58,975.301	-0.8261	Fermi GBM
59,142.251	-0.8640	Swift BAT
59,339.195	-0.6984	MAXI
59,659.037	-0.8285	Fermi GBM
59,805.990	-0.9832	Swift BAT
59,939.781	-1.1869	MAXI
60,149.720	-0.9594	MAXI

**Figure 5.** Evolution of superorbital phases folded by the CG01 ephemeris from 1987 to 2023. The dotted, solid and dashed lines represent the best fits for linear, glitch and quadratic models, respectively. The shaded area indicates the low power state between MJD 50,773 and 52,627, and the vertical dash-dot line represents the glitch time MJD $52,380 \pm 414$ evaluated by the glitch model, with the horizontal error bar indicating the 1σ uncertainty of the glitch time.

the root-mean deviation (RMSD), defined as:

$$RMSD \equiv \sqrt{\frac{1}{\nu} \sum_{i=1}^N [\phi_i - \phi(t_i)]^2} \quad (4)$$

where ϕ_i is the detected phase, $\phi(t_i)$ is the expected phase value at t_i evaluated from the best fit model, and ν is the degree of freedom. The RMSD is 0.12 for the linear model. However best-fitted period in this model significantly differs from the reported superorbital periods that were detected in early RXTE ASM observations, as listed in Table 5, as well as the superorbital period of 176.4 ± 1.3 days reported by [Priedhorsky & Terrell \(1984\)](#) from Vela 5B observation. Furthermore, the expected phase at the midpoint of Ginga ASM observation time (MJD 47,677.56) is 0.426 ± 0.047 , about 6.9σ different from the detected value of 0.104 (see Figure 5). Therefore, the linear model is unlikely to describe the superorbital phase evolution of 4U 1820-30.

3.2.2. Glitch Model

Table 5 presents the reported superorbital periods detected by early RXTE ASM observations, which are roughly consistent with the period in the CG01 ephemeris (171 days). However, for later observations, particularly those from Swift BAT, MAXI, and Fermi GBM the period is approximately 167.4 days, as listed in Table 1. One the possibility is that the superorbital

Table 4. Parameters of Superorbital Modulation of 4U 1820-30

Linear model	
$\phi = a_0 + a_1(t - T_0)$	
$a_0 = (T_0 - T_{0,CG01})/P_{CG01}$ ^a	
$a_1 = (P_0 - P_{CG01})/(PP_{CG01})$	
Parameter	Value
a_0	0.084 ± 0.030
a_1 (cycle/day)	$(-1.058 \pm 0.056) \times 10^{-4}$
$cov(a_0, a_1)$ (cycle/day)	-1.43×10^{-7}
T_0 (MJD)	$50,923.72 \pm 5.19$
P (days)	167.99 ± 0.16
Glitch model	
$\phi = \begin{cases} a_0 + a_1(t - T_0) & \text{if } t \leq T_g; \\ a'_0 + a'_1(t - T_0) & \text{if } t > T_g. \end{cases}$	
$a_0 = (T_0 - T_{0,CG01})/P_{CG01}$	
$a_1 = (P_1 - P_{CG01})/(P_1P_{CG01})$	
$a'_0 = (T_0 - T_{0,CG01})/P_{CG01} + n_g(P_1 - P_2)/P_2$	
$a'_1 = (P_2 - P_{CG01})/(P_2P_{CG01})$	
$T_g = T_0 + n_gP_1$	
Parameter	Value
a_0	0.034 ± 0.027
a_1 (cycle/day)	$(-9.12 \pm 19.29) \times 10^{-6}$
$cov(a_0, a_1)$ (cycle/day)	-8.47×10^{-8}
a'_0	0.205 ± 0.043
a'_1 (cycle/day)	$(-1.260 \pm 0.071) \times 10^{-4}$
$cov(a'_0, a'_1)$ (cycle/day)	-2.82×10^{-7}
T_0 (MJD)	$50,915.27 \pm 4.60$
P_1 (days)	170.77 ± 0.56
P_2 (days)	167.43 ± 0.20
n_g	8.58 ± 3.19
T_g (MJD)	$52,379 \pm 414$
Quadratic model	
$\phi = a_0 + a_1(t - T_0) + a_2(t - T_0)^2$	
$a_0 = (T_0 - T_{0,CG01})/P_{CG01}$	
$a_1 = (P_0 - P_{CG01})/(P_0P_{CG01})$	
$a_2 = 1/2 \dot{P}/(P_0P_{CG01})$	
Parameter	Value
a_0	0.032 ± 0.025
a_1 (cycle/day)	$(-4.77 \pm 1.08) \times 10^{-5}$
a_2 (cycle/day ²)	$(-7.24 \pm 1.24) \times 10^{-9}$
$cov(a_0, a_1)$ (cycle/day)	-1.71×10^{-7}
$cov(a_0, a_2)$ (cycle/day ²)	1.10×10^{-11}
$cov(a_1, a_2)$ (cycle ² /day ³)	-1.24×10^{-14}
T_0 (MJD)	$50,914.92 \pm 4.24$
P_0 (days)	169.65 ± 0.31
\dot{P} (day/day)	$(-4.20 \pm 0.72) \times 10^{-4}$
\dot{P}/P_0 (yr ⁻¹)	$(-9.04 \pm 1.55) \times 10^{-4}$

^a $T_{0,CG01} = \text{JD } 2,450,909.9 = \text{MJD } 50,909.4$ and $P_{CG01} = 171.033$ days from Eq.9 of GC01.

Table 5. Superorbital periods of 4U 1820-30 from Early RXTE ASM Observations^a

Observation Time (MJD)	Period (days)	Reference
50,088-51,606	171.39 ± 1.93 ^b	CG01
50,088-52,350	172.78	Šimon (2003)
50,088-53,243	172 ± 1	Wen et al. (2006)
50,088-54,151	170.6 ± 0.3	Zdziarski et al. (2007a)

^aRXTE ASM was operated from MJD 50088 to 55831

^bThe period of local ephemeris from Eq.8 in CG01.

period underwent an abrupt change (glitch), likely between years 2000 and 2005 (see Figure 5).

On the other hand, Kotze & Charles (2012) conducted a dynamic power spectrum analysis and observed weaker superorbital modulation power during the period MJD 51,200-52,200, hereafter, referred to as the low power state. Additionally, signals with shorter periods, ~ 85 days (second harmonic) and ~ 65 days emerged in the dynamic power spectrum, indicating a change in the modulation profile during that time interval. However, considering the window size used to generate the dynamic power spectrum of 4U 1820-30 in Kotze & Charles (2012) (5 cycles), this low power state time interval should be extended to approximately MJD 50,773 to 52,627.

Compared with the phase evolution (i.e. Figure 5), it appears likely that the glitch occurred around MJD 52,500, near the end of low power state. Marginal evidences support this assumption. As listed in Table 5, the reported superorbital period by Zdziarski et al. (2007a) was 170.6 ± 0.3 days, slightly smaller than those reported by CG01, Šimon (2003), and Wen et al. (2006). This discrepancy may be due to that a significant portion of data ($\sim 37\%$) analyzed by Zdziarski et al. (2007a) were collected after MJD 52,500. Similarly, the power spectral analysis of the entire RXTE ASM light curve yielded a superorbital period of 169.09 days (see Table 1), falling between 171 and 167.4 days, because about half ($\sim 56\%$) of the data were collected after MJD 52,500. Conversely, the periods detected from the power spectra of Swift BAT, MAXI, and Fermi GBM were at approximately 167 days, because these observations were made after MJD 52,500 (see Table 1).

We therefore fitted the phase evolution with the glitch model using the ephemeris described by Eq.5 in (Wolff et al. 2009)

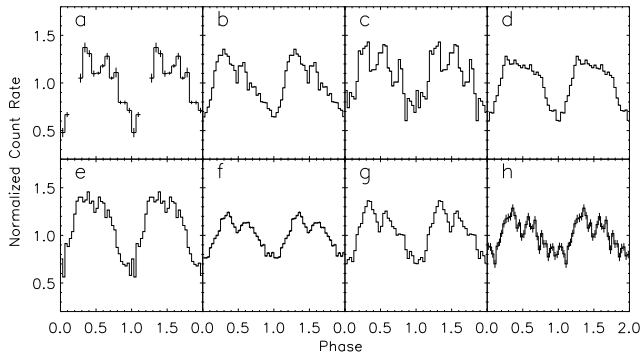


Figure 6. Superorbital modulation profiles folded by glitch ephemeris listed in Table 4 for the light curves collected by (a) Ginga ASM, (b) RXTE ASM, before glitch, (c) RXTE PCA, before glitch, (d) RXTE ASM, after glitch, (e) RXTE PCA, after glitch, (f) Swift BAT, (g) MAXI, and (h) Fermi GBM.

$$T_N = \begin{cases} T_0 + P_1 N & \text{if } N \leq n_g; \\ T_0 + P_1 n_g + P_2 (N - n_g) & \text{if } N > n_g. \end{cases} \quad (5)$$

where T_0 is the phase zero epoch, P_1 and P_2 are the periods before and after the glitch, respectively, n_g is the glitch cycle count, and the glitch time $T_g \equiv T_0 + P_1 n_g$. The fitting results are shown in Figure 5, and the parameters are listed in Table 4. We obtained significantly different superorbital periods of 170.77 ± 0.56 days and 167.43 ± 0.20 days before and after the glitch time $\text{MJD } 52,379 \pm 414$, which occurred approximately between early 2001 and mid-2003, respectively. The change in the superorbital period is given by $\Delta P_{sup}/P_{sup} = -0.028 \pm 0.003$. The RMSD for this glitch model is 0.089. Comparing this with the RMSD of 0.12 from the linear model, the F-test yielded a p-value of 0.04, indicating that the glitch model is better than the linear model. Figure 6 shows the modulation profiles folded by the glitch ephemeris. All the superorbital minima (fiducial points) are close phase zero, implying that this ephemeris effectively describes the superorbital phase evolution of 4U 1820-30 from 1987 to 2023.

3.2.3. Quadratic Model

While the glitch model effectively describes the superorbital phase evolution, we cannot rule out the possibility that period difference between early RXTE ASM observations and recent ones stems from a smooth change in the superorbital period. Farrell et al. (2009) observed

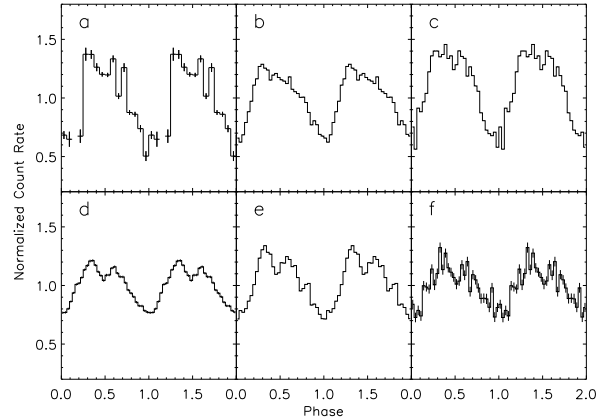


Figure 7. Superorbital modulation profiles folded by quadratic ephemeris listed in Table 4 for the light curves collected by (a) Ginga ASM, (b) RXTE ASM, (c) RXTE PCA, (d), Swift BAT, (e) MAXI, and (f) Fermi GBM.

that the peak width of the superorbital signal in the power spectrum made from RXTE ASM and Swift BAT light curves were marginally wider than that from simulations, suggesting that a change in superorbital period. Hence, we apply a simple model assuming a constant period derivative (\dot{P}_{sup}) to fit a quadratic function to the superorbital phase evolution. The fitting results are depicted in Figure 5, and the parameters are listed in Table 4. A period derivative of $\dot{P}_{sup} = (-4.20 \pm 0.72) \times 10^{-4}$ day/day, or $\dot{P}_{sup}/P_{sup} = (-9.04 \pm 1.55) \times 10^{-4} \text{ yr}^{-1}$ was obtained from the fitting, and a quadratic ephemeris

$$T_N = (\text{MJD} 50,914.92 \pm 4.24) + (169.65 \pm 0.31) \times N + (-3.56 \pm 0.62) \times 10^{-2} \times N^2 \quad (6)$$

was established. The RMSD for the quadratic model is 0.087. Compared to this with the RMSD of 0.089 from glitch model, the F-test yielded a p-value of 0.55, which indicating that these two models are about equally adept at describing the superorbital phase evolution. Figure 7 illustrates the modulation profiles folded by the quadratic model. Similar to the glitch model, all the superorbital minima (fiducial points) are located around phase zero. It provides an evidence that the quadratic model is suitable for describing the superorbital phase evolution of 4U 1820-30.

3.3. X-ray Burst Active Times

As previously mentioned in Section 1, Type-I X-ray bursts of 4U 1820-30 are exclusively observed during the low state (Clark et al. 1977; Stella et al. 1984). Further confirmed by CG01, indicated the Type-I X-ray

bursts were detected only within ± 23 days around superorbital minima for bursts reported before 1985. This supports the hypothesis that the superorbital modulation stems from changes in the accretion rate changes rather than occultation effects. However, CG01’s statistics only included four burst active dates. Subsequently, more X-ray bursts of 4U 1820-30 were detected. With the updated superorbital ephemerides, this evidence can be further substantiated. Although the possibility exists that the X-ray bursts occur in another low state, which may deviate significantly from the superorbital minima (e.g. the brief low state (BLS) found by Šimon (2003)), it is likely that the most of X-ray burst active times would cluster around the superorbital minima.

In this study, we collected the reported burst active dates of 4U 1820-30 from Grindlay et al. (1976); Vacca et al. (1986); Haberl et al. (1987); Zdziarski et al. (2007b); García et al. (2013), and (Yu et al. 2024), as well as four superbursts discovered by Strohmayer & Brown (2002); in’t Zand et al. (2011); Serino et al. (2021a), and Serino et al. (2021b). The deviations in burst active dates relative to the nearest superorbital minima predicted by CG01 and three ephemerides derived in this study are shown in Figure 8. It is evident that large deviations can be observed after the low power state (MJD $\sim 52,672$) when using the superorbital minima predicted by the CG01 ephemeris. The root-mean-square deviations are 41.2, 33.5, 27.3 and 26.7 days for CG01, linear, glitch and quadratic ephemerides, respectively. This provides supportive evidence that glitch and quadratic ephemerides are better than CG01 and linear ephemerides in describing the superorbital phase evolution of 4U 1820-30. Notably, X-ray bursts occurring between MJD 50,339 and MJD 50,343 exhibited large deviations (~ 60 days) for all ephemerides. Upon examining the RXTE ASM light curve, we observed that these X-ray bursts occurred around a BLS with a count rate of only 12.0 cts/s compared to the mean count rate of 21.0 cts/s. This observation reaffirms that superorbital modulation is primarily caused by accretion variations rather than occultation effects.

On the contrary, out of the four superbursts detected, only the one on MJD 51,430 (Strohmayer & Brown 2002) fell within ± 23 days region, whereas the other three occurred outside of this timeframe for both glitch and quadratic ephemerides (see Figure 8). Upon examining the RXTE ASM and MAXI light curves, we observed that the count rates on the dates of superbursts were 57%, 150%, 121% and 138% of the corresponding mean count rates of the light curves for the superbursts detected

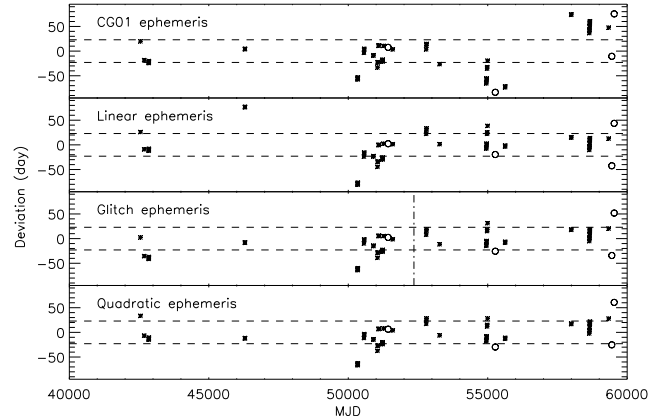


Figure 8. The deviations of Type-I X-ray burst active dates relative to the nearest expected superorbital minima evaluated by CG01, linear, glitch and quadratic ephemerides. The circles are the superbursts reported by Strohmayer & Brown (2002); in’t Zand et al. (2011); Serino et al. (2021a,b). The region between two horizontal dashed lines is the ± 23 days burst active interval suggested by CG01, and the vertical dash-dotted line in the plot of glitch ephemeris is the glitch time evaluated by the glitch model (Section 3.2.2).

on MJD 51,430 (Strohmayer & Brown 2002), MJD 55,272 (in’t Zand et al. 2011), MJD 59,449 (Serino et al. 2021a) and MJD 59,543 (Serino et al. 2021b), respectively. It is likely that the low state constraint for the regular X-ray bursts of 4U 1820-30 (Clark et al. 1977; Stella et al. 1984) does not apply to the superbursts. More observations are required for further confirmation.

4. DISCUSSION

4.1. Challenge of the Triple Model

The initial aim of this study was to further validate the stability of superorbital period of 4U 1820-30, a crucial piece of evidence for the triple model as described in Section 1, which explains its superorbital modulation with a period of ~ 170 days. Given that 4U 1820-30 resides in NGC 6624, a star-crowded region, previous studies suggested a high likelihood of the binary capturing a third star and forming a stable hierarchical triple system (Grindlay 1988). Black (1982) proposed a stability criterion for such a triple system as

$$\mu \leq \mu_{crit} = 0.175 \frac{\Delta^3}{(2 - \Delta)^{3/2}} \quad (7)$$

where $\mu = (m_2 + m_3)/2m_1$, $\Delta = 2(R - 1)/(R + 1)$, $R = R_3/R_1$, m_1 , m_2 and m_3 are the masses of binary primary, secondary and tertiary companion, respectively, R_1 is the binary separation and R_3 is the maximum separation of the binary primary and the ter-

tiary companion. Applying Eq. 7 to 4U 1820-30 system with the assumption that $m_1 = 1.4M_\odot$, $m_2 = 0.07M_\odot$ (Chou & Jhang 2023), $m_3 = 0.5M_\odot$ (CG01), binary period of 685 s and third star orbital period of 1.1 days (see Section 1), according to the Kepler's third law, we found that $\mu = 0.204$ and $\mu_{crit} = 24.18$, which satisfies the stability criterion proposed by Black (1982). Additionally, CG01, based on their analysis of the RXTE ASM light curve collected between 1996 and early 2000 and in conjunction with fiducial points measured by Vela 5B and Ginga, found no significant superorbital period derivative, setting an upper limit of $|\dot{P}_{sup}/P_{sup}| < 2.2 \times 10^{-4} \text{ yr}^{-1}$, thereby confirming its stability and lending support to the triple model. Therefore, for the 4U 1820-30 system, with additional subsequent observations after 2000, one would expect that the observed superorbital period would closely match the value found by CG01 (171 days) and that the period derivative could be further constrained.

However, upon analyzing X-ray light curves collected by the sky monitoring/scanning instruments from 1987 to 2023, we discovered a significant change in the superorbital period from 171 days to 167 days, identified through both power spectral analysis (Section 3.1) and phase analysis (Section 3.2) over a time span of ~ 36 years. This suggests that the ephemeris proposed by CG01 is no longer suitable for describing the superorbital modulation of 4U 1820-30, and the period is not as stable as anticipated by triple model. By analyzing the superorbital phase evolution, we suggested that the superorbital period may have experienced an abrupt change during early 2001 to mid-2003 ($T_g = MJD52,379 \pm 414$) or may be constantly changing with a period derivative of $\dot{P} = (-4.20 \pm 0.72) \times 10^{-4} \text{ day/day}$.

The significant difference between the period detected from Vela 5B observation, 176.4 ± 1.3 days (Priedhorsky & Terrell 1984), and Ginga observation, 171.12 ± 1.99 days (see Table 1) suggests that the superorbital period may have experienced another glitch between 1976 and 1987. If 4U 1820-30 is a hierarchical triple system, from Eq. 1, a glitch in superorbital period may be induced by changes in either the binary orbital period or the third star orbital period as

$$\frac{\Delta P_{sup}}{P_{sup}} = 2 \frac{\Delta P_3}{P_3} - \frac{\Delta P_{orb}}{P_{orb}} \quad (8)$$

Glitches in orbital periods have been observed in some LMXBs that exhibit total eclipses, such as EXO 0748-676 (Wolff et al. 2009), XTE J1710-281 (Jain & Paul 2011; Jain et al. 2022), and AX J1745.6-2901 (Ponti et al. 2017). These glitches likely result from magnetic, solar-type cycles of the compan-

ion star, affecting the mass distribution of companion and leading to variations in its quadrupole moment (Wolff et al. 2009). However, the magnitudes of these glitches are typically in the order of milliseconds, with $\Delta P_{orb}/P_{orb} \sim 10^{-7} - 10^{-6}$. For 4U 1820-30 system, the superorbital period glitch was measured as $|\Delta P_{sup}/P_{sup}| = 2.8 \times 10^{-2}$. No glitch has ever been observed in the binary orbital phase evolution (see Figure 4 in Chou & Jhang 2023), implying that the orbital period glitch of the third companion was as high as $|\Delta P_3/P_3| = 1.4 \times 10^{-2}$, about 4 orders of magnitude larger than those from eclipsing LMXBs. However, the superorbital period change may not occur abruptly but within a finite short time interval. Suppose the timescale to be 800 days, estimated from the uncertainty of T_g , the mean orbital period derivative of the third star would be as high as $|\dot{P}_3| \approx 4 \times 10^{-3} \text{ day/day}$. Thus, the triple model is unlikely to explain this large superorbital period change in such a short time.

The low power state is a particular phase during the superorbital modulation evolution of 4U 1820-30. The dynamic power spectrum demonstrated in Figure 24 of Kotze & Charles (2012) indicates that in addition to the weaker power detected in the superorbital period, the powers of its second harmonic and a signal of period ~ 65 days became significant. This suggests that the modulation was more complicated than usual. Our phase analysis results also show that the superorbital phases had larger fluctuation during the low power state (see Figure 5) with an RMSD of 0.11, evaluated by the best glitch model fitting, compared to 0.075 for the phases outside low power state. It is probable that the superorbital period was 171 days before the low power state, became unstable during the low power state, and stabilized at 167 days later. However, it is unclear what the cause of this phenomenon is.

Furthermore, from the phase evolution illustrated in Figure 5, we observed that the phase fluctuation increased significantly after MJD $\sim 58,000$. The RMSD value, calculated at 0.13 using the best glitch model fitting, aligns with the value observed during the low power state. It suggested that 4U 1820-30 may be entering another low power state. To confirm this hypothesis, we generated a dynamic power spectrum of the light curve collected by MAXI as shown in Figure 9, using the same method as the one proposed by Kotze & Charles (2012). Notably, a decrease in power is evident after MJD $\sim 59,000$. Considering the window size of five cycles, the onset of the new low power state is estimated to be around MJD 58,600. By comparing the start time of low power state observed in early RXTE ASM observation (MJD $\sim 50,773$), the recurrent time of

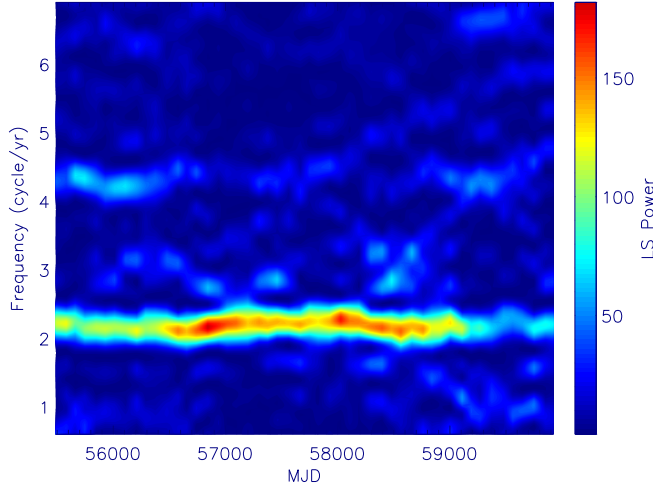


Figure 9. The dynamic power spectrum generated from the light curve collected by MAXI. The power of superorbital modulation with a frequency ≈ 2.18 cycles/year was evidently lower after MJD $\sim 59,000$. This implies that the 4U 1820-30 has entered a new low power state.

this phenomenon is about 21.3 years. If the durations of these two low power states are roughly equivalent ($\sim 1,860$ days), the new low power state is expected to end on about MJD 60,460, corresponding to 2024 May 30. Additional observations over the next a few years will enable us to confirm this prediction and verify the presence of a superorbital period glitch in this new low power state. Moreover, if this phenomenon is periodically recurrent, the low power state preceding the one observed in early RXTE observation would likely have commenced around MJD 42,950, near the end of Vela 5B data period analyzed by [Priedhorsky & Terrell \(1984\)](#) (mid of 1976), and end around MJD 44,800, before start time of Ginga ASM light curve (MJD 46,860). There may have been a superorbital period glitch causing the period change from 176.4 days to 171 days during this period.

Conversely, the superorbital phase evolution is also well-fitted by a quadratic model, although there is a significant difference (1.8σ) between the period evaluated as ephemeris extrapolated to the midpoint of Vela 5B observation time (173.54 ± 0.97 days) and the observed period (176.4 ± 1.3 days) as reported by [Priedhorsky & Terrell \(1984\)](#). If 4U 1820-30 were a hierarchical triple system, from Eq. 1, the relation of period derivatives could be written as

$$\frac{\dot{P}_{sup}}{P_{sup}} = 2\frac{\dot{P}_3}{P_3} - \frac{\dot{P}_{orb}}{P_{orb}} \quad (9)$$

Although the exact binary orbital period derivative is unknown, it is believed it is $\dot{P}_{orb}/P_{orb} \sim +10^{-7}$

yr^{-1} ([Chou & Jhang 2023](#)). Therefore, the observed superorbital period derivative $\dot{P}_{sup}/P_{sup} = (-9.04 \pm 1.55) \times 10^{-4} \text{ yr}^{-1}$ is contributed by the tertiary companion, with a value of $\dot{P}_3/P_3 = -4.5 \times 10^{-4} \text{ yr}^{-1}$, corresponding to a variation timescale of only $\sim 2,200$ years. From Eq. 7, we infer that the triple system should be stable; therefore, such a fast period change is unlikely to occur. Furthermore, the acceleration from the gravitational potential in NGC 6624, estimated as $a_c/c \sim -10^{-7} \text{ yr}^{-1}$ ([Peuten et al. 2014](#)), is insufficient for the orbital period derivative of the third companion derived from Eq. 9. Thus, the triple model can hardly explain the observed superorbital period derivative.

If 4U 1820-30 is not a triple system, the constraints regarding the observed value of the binary orbital period derivative may be relaxed. To explain the discrepancy between the positive theoretical value ($\dot{P}_{orb}/P_{orb} > 8.8 \times 10^{-8} \text{ yr}^{-1}$, [Rappaport et al. 1987](#)) and the negative observed value ($\dot{P}_{orb}/P_{orb} = (-5.21 \pm 0.13) \times 10^{-8} \text{ yr}^{-1}$, [Chou & Jhang 2023](#)) of the binary orbital period derivative, it has been proposed that 4U 1820-30 is being accelerated by the gravitational potential within the globular cluster NGC 6624 ([Tan et al. 1991](#); [Peuten et al. 2014](#)). However, [Peuten et al. \(2014\)](#) suggested that the maximum radial acceleration from the gravitational potential from NGC 6624 itself ($|a_{c,max}/c| = 1.3 \times 10^{-9} \text{ yr}^{-1}$) is an order of magnitude smaller than the value required to explain the observed binary period derivative. Therefore, [Peuten et al. \(2014\)](#) proposed three possible scenarios to provide additional acceleration for 4U 1820-30, a flyby stellar mass dark remnant, an intermediate-mass black hole at the center of NGC 6624, and a central concentration of dark remnants. Only the last scenario was preferred because the first two scenarios tend to destroy the triple system ([Peuten et al. 2014](#)). However, if 4U 1820-30 is a pure binary system, the first two scenarios become viable explanations for the observed binary orbital period derivative.

4.2. Thermal Disk Instability

The fact that the type-I X-ray bursts of 4U 1820-30 can only be observed in the low state ([Clark et al. 1977](#); [Stella et al. 1984](#)) has been reconfirmed in this work (see Section 3.3). This implies that the superorbital modulation of 4U 1820-30 is caused by variations in accretion rate rather than by external absorption or precession of accretion disk. [Kotze & Charles \(2012\)](#) listed eight possible mechanisms to account for the superorbital modulations observed in X-ray binaries, but only the third body (i.e., triple model) and the X-ray state changes can possibly be responsible for the superorbital modulation of 4U 1820-30. If the triple

model is ruled out due to the instability of superorbital period, the only remaining mechanism is the X-ray state changes. X-ray state changes refer to variations in mass accretion rate between high and low states due to thermal disk instability, as observed in dwarf novae and soft X-ray transients. [Priedhorsky & Terrell \(1984\)](#) proposed that this mechanism could explain for the superorbital modulation of 4U 1820-30. However, [Menou et al. \(2002\)](#) pointed out that if thermal disk instability could occur in 4U 1820-30 system, the mass transfer rate $\dot{m} \leq \dot{m}_{crit} = 4.4 \times 10^{16} \text{ g s}^{-1}$. From the mean flux of $\langle F_{bol} \rangle = 8.7 \times 10^{-9} \text{ erg cm}^{-2} \text{ s}^{-1}$ for 4U 1820-30 ([Zdziarski et al. 2007b](#)) and the distance of $8.019^{+0.108}_{-0.107} \text{ kpc}$ for NGC 6624 ([Baumgardt & Vasiliev 2021](#)), we obtained a mean luminosity of $\langle L \rangle = 6.7 \times 10^{37} \text{ erg s}^{-1}$ and a mass accretion rate of $\dot{m}_1 = 3.6 \times 10^{17} \text{ g s}^{-1}$ for a neutron star with a mass of $1.4 M_\odot$ and a radius of 10^6 cm . It is approximately an order of magnitude larger than the \dot{m}_{crit} . Therefore, this mechanism is unlikely to explain the superorbital modulation of 4U 1820-30.

4.3. Irradiation-induced Mass Transfer Instability

[Zdziarski et al. \(2007b\)](#) discovered that the binary orbital modulation amplitude and the offset phase in 4U 1820-30 depend significantly on the accretion rate, which is highly related to the superorbital modulation phase. The orbital modulation in the X-ray band is believed to be caused by absorption from structures in the disk rim where the accretion flow from the companion impacts the outer edge of the disk ([Stella et al. 1987](#)). As the mass loss rate changes, variations of the accretion stream induce changes in the absorption of outer edge structures and the position of impact point. This makes the amplitude and phase of orbital modulation dependent on the mass loss rate, and subsequently, on the accretion rate after a viscous time of $\sim 10^5 \text{ s}$ ([Zdziarski et al. 2007b](#)). The variation in mass loss rate could be explained by the triple model as described in Section 1, where the eccentricity variation of the binary system induced by the third companion result in changes to the mass loss rate. Although the superorbital modulation is probably not a consequence of a third companion, the discovery by [Zdziarski et al. \(2007b\)](#) implies that the superorbital modulation of 4U 1820-30 is due to changes in mass loss rate.

One possible cause of variations in the accretion flow, aside from the presence of a third companion, is irradiation-induced mass transfer instability. This model has proposed to explain the flux variation of soft X-ray transients ([Hameury et al. 1986](#)) and was included into the hybrid model proposed by [Simon \(2003\)](#).

Due to small binary separation of 4U 1820-30, the irradiation on the companion by the X-ray emission from the neutron star and the inner part of accretion disk is strong. Because the companion of 4U 1820-30 is only partially degenerate ([Rappaport et al. 1987](#)), irradiation on the non-degenerate envelope enhances the mass loss of the companion. [Chou & Jhang \(2023\)](#) estimated that at least 40% of the mass lost from the companion is ejected from the binary system. Such a strong outflow is probably caused by the irradiation on the companion, as proposed by [Tavani \(1991\)](#). However, part of X-ray irradiation on the companion is blocked by the accretion disk, with the area that depending on the scale height of the disk rim. When the scale height of disk rim is small, a larger irradiation area enhances the mass loss rate and the accretion flow, which increases the scale height of the accretion disk rim. Conversely, when the scale height of accretion disk rim is large, a larger portion of the companion's surface is shielded by the disk. This results in a reduction in the mass loss rate, as well as in the accretion flow and the scale height of the accretion disk rim. This cyclical process may explain the quasi-periodic superorbital modulation of 4U 1820-30.

Suppose the accretion disk in 4U 1820-30 is geometrically thin and optically thick ([Pringle 1981](#)). The shielded region on the companion can be estimated. For 4U 1820-30 with a neutron star mass of $m_1 = 1.4M_\odot$, a companion mass of $m_2 = 0.07M_\odot$ ([Chou & Jhang 2023](#)), and an orbital period of $P_{orb} = 685 \text{ s}$, we derived the binary separation of $a = 1.33 \times 10^{10} \text{ cm}$ from Kepler's third law. The discovery of the superhump in 4U 1820-30 system ([Wang & Chakrabarty 2010](#)) indicates that the rim of the accretion disk reaches a 3:1 resonance radius, giving a disk radius of $r_d = 6.4 \times 10^9 \text{ cm}$. The scale height of the accretion disk can be evaluated as $\sqrt{kT/\mu m_H}/\Omega_k$ ([Spruit 2010](#)) where T and Ω_k are the temperature and the Keplerian angular velocity at the disk radius r , m_H is the mass of a hydrogen atom, $\mu = 4$ for a helium-dominated disk, and k is the Boltzmann constant. The temperature at the disk rim is estimated as

$$T = \left(\frac{3G\dot{m}_1 m_1}{8\pi\sigma r_d^3} \right)^{\frac{1}{4}} \quad (10)$$

([Pringle 1981](#)) where σ is Stefan-Boltzmann constant and G is gravitational constant. The accretion rate of 4U 1820-30 $\dot{m}_1 = 3.6 \times 10^{17} \text{ g s}^{-1}$. Thus, the temperature at the disk rim is $T = 2.7 \times 10^4 \text{ K}$ and the scale height is $H = 2.8 \times 10^7 \text{ cm}$. For a Roche lobe filling companion, the radius of companion is $R_2 = R_L = 2/3^{4/3}[q/(1+q)]^{1/3}a$ ([Paczynski 1971](#)) where $q = m_2/m_1$. For 4U 1820-30 system, $q=0.05$, so

$R_2 = 1.68 \times 10^9$ cm. The scale height of the irradiation shielded by the accretion disk on the companion around L_1 point is $h = H(a - R_2)/r_d = 5.0 \times 10^7$ cm, which is equivalent to a latitude of $\sin^{-1}(h/R_2) = 1.7^\circ$ on the companion surface. Although the shielded latitude is small, it covers the L_1 point if the orbital plane and the accretion disk are coplanar. The accretion stream flows from a small region around the L_1 point on the surface of companion. If the accretion disk rim partially obscures this region, even a marginal change in irradiation on this region due to variations in the scale height of accretion disk rim could induce a significant change in mass loss because of the weak effective gravitational field around the L_1 point. Such a large variation in mass loss rate could result in quasi-periodic superorbital modulation, causing a 2-3 fold change in the X-ray flux of 4U 1820-30. However, more observations and theoretical studies are required to verify this irradiation-induced mass transfer instability scenario, including the evolution of superorbital period discovered in this study.

5. CONCLUSION

The triple model was once considered a plausible explanation for the superorbital modulation observed in 4U 1820-30. The stability of the superorbital period is the crucial evidence for verifying this model. CG01 suggested that the superorbital period was stable at 171 days and early RXTE ASM data support this 171-day periodicity, indicating stability of superorbital period.

In this study, we analyzed the data collected by Ginga ASM, RXTE ASM, RXTE PCA, Swift BAT, MAXI, and Fermi GBM over a time span of 36 years to verify the triple model for the 4U 1820-30 system. The superorbital periods derived from the power spectra of these six instruments show a significant change from 171 days to 167 days between 1987 and 2023, suggesting the instability of the superorbital period. Phase analysis revealed that the superorbital period may have experienced a period glitch between early 2001 and mid-2003, or may have changed smoothly with a period derivative of $\dot{P}_{sup} = (-4.20 \pm 0.72) \times 10^{-4}$ day/day. Two ephemerides, glitch and quadratic, were established to describe the expected superorbital minimum times of 4U 1820-30. These updated ephemerides accurately describe the superorbital minimum times with a mean phase jitters of ~ 0.08 cycles. The fact that the Type-I X-ray bursts can be observed only in the low state implies a high probability of detecting the bursts around the superorbital minimum. By examining previously reported burst detection dates with different ephemerides, we found that the burst dates are more clustered around the superorbital phase zero when folded with the glitch

and quadratic ephemerides, rather than with linear and CG01 ephemerides. This is not only reconfirms the low state constraint for regular X-ray bursts as suggested by Clark et al. (1977) and Stella et al. (1984), but also provides supportive evidence that the glitch and quadratic ephemerides are better to describe the superorbital minimum times.

The instability of the superorbital periodicity in 4U 1820-30 discovered in this work seriously challenges the triple model. If the triple model were applicable to 4U 1820-30 system, according to Eq. 1, the superorbital period change could be due to either the binary period variation or the orbital period change of the third companion. However, the binary orbital modulation has been monitored for over 46 years, and neither a period glitch nor a large period derivative of $\dot{P}_{orb}/P_{orb} \sim 10^{-4}$ yr $^{-1}$ had previously been observed (see Chou & Jhang 2023). Therefore, the superorbital period changes likely reflect the orbital period variation of the third companion. While orbital period glitches have been observed in some eclipsing LMXBs, the magnitude of these change is much smaller than that the superorbital period glitch observed 4U 1820-30. The period derivative derived from the quadratic model indicates that the timescale of the orbital period evolution of the third companion is ~ 2200 years, which is inconsistent with the expected stability in a hierarchical triple system. If the triple model does not apply to the 4U 1820-30 system, two previously unfavorable scenarios proposed by Peuten et al. (2014) - a stellar mass dark remnant and an intermediate mass black hole - can be reconsidered to explain the discrepancy between the theoretical and observed binary orbital period derivatives.

The absence of regular Type-I bursts in the high state suggests that the superorbital modulation of 4U 1820-30 results from variations in the accretion rate rather than from the occultation effect caused by the precession of a tilting or warping accretion disk. Thermal disk instability is unlikely to be the cause of the superorbital modulation due to the high accretion rate of 4U 1820-30. On the other hand, because the amplitude of orbital modulation highly depends on accretion rate (Zdziarski et al. 2007b), the superorbital modulation could result from variation in mass transfer from the companion. Given the change in superorbital period of 4U 1820-30, such variation is unlikely to be induced by a third companion. We proposed that irradiation-induced mass transfer instability may be responsible for the superorbital modulation of 4U 1820-30. The accretion stream is expected to flow from a small region around the L_1 point on companion, where the effective gravitational field is weak. Therefore, the accretion stream is highly sensitive

to the X-ray irradiation of this region. The irradiation onto this region may be partly blocked by the accretion disk rim, whose scale height also depends on the accretion stream. Small variations in the scale height can lead to significant changes in accretion stream. A cyclical process could result in quasi-periodic superorbital modulation in 4U 1820-30.

Using the data collected by X-ray monitoring/scanning X-ray telescopes, we discovered the instability of the superorbital period of 4U 1820-30. From our study, we found that both the glitch model and the quadratic model describe the superorbital phase evolution well. However, additional observations are necessary to validate these models or to provide a better ephemeris for the superorbital modulation of 4U 1820-30. This period instability suggests that the triple model is unlikely suitable to explain the superorbital modulation of 4U 1820-30. Although we propose that the irradiation-induced mass transfer instability may be responsible for the superorbital modulation, further observations and theoretical works are required to verify this model, including the periodicity, modulation amplitude and profile, and the puzzling phase evolution, which were identified in this study. Fortunately, Swift BAT, MAXI and Fermi GBM continue to monitor the X-ray sky. Additionally, the newly operational Wide-field X-ray Telescope on-board the Einstein

Probe (Yuan & Osborne 2015), which is sensitive to 0.5 to 4.0 keV X-ray photons and scans the entire night sky in three satellite orbits, can provide further data to better understand the nature of the superorbital modulation of 4U 1820-30.

The authors thank the anonymous referee for valuable suggestions that improved the manuscript. J.-L.W. and B.-C.C. especially acknowledge the support from the National Science and Technology Council of Taiwan through the grant NSTC 113-2112-M-008-002. This research has made use of data and software provided by the High Energy Astrophysics Science Archive Research Center (HEASARC), which is a service of the Astrophysics Science Division at NASA/GSFC. We also express our gratitude to the RXTE team for archiving the RXTE PCA monitoring observations of the galactic center and plane data, to Swift BAT transient monitor team for archiving the Swift BAT data, to MAXI team for archiving the MAXI data, and to Gamma-Ray Astrophysics Team of NSSTC for archiving the Fermi GBM data.

Facilities: ADS, HEASARC, Ginga (ASM), RXTE (ASM), RXTE (PCA), Swift (BAT), MAXI, Fermi (GBM)

Software: heasoft(v6.31:Nasa High Energy Astrophysics Science (Heasarc)), Astropy(Astropy Collaboration et al. (2013, 2018))

REFERENCES

- Astropy Collaboration, Robitaille, T. P., Tollerud, E. J., et al. 2013, *A&A*, 558, A33.
doi:10.1051/0004-6361/201322068
- Astropy Collaboration, Price-Whelan, A. M., Sipőcz, B. M., et al. 2018, *AJ*, 156, 123. doi:10.3847/1538-3881/aabc4f
- Barthelmy, S. D., Barbier, L. M., Cummings, J. R., et al. 2005, *SSRv*, 120, 143. doi:10.1007/s11214-005-5096-3
- Baumgardt, H. & Vasiliev, E. 2021, *MNRAS*, 505, 5957.
doi:10.1093/mnras/stab1474
- Black, D. C. 1982, *AJ*, 87, 1333. doi:10.1086/113220
- Chou, Y. & Grindlay, J. E. 2001, *ApJ*, 563, 934. (CG01)
doi:10.1086/324038
- Chou, Y. & Jhang, Y.-W. 2023, *ApJ*, 951, 42.
doi:10.3847/1538-4357/acd376
- Clark, G. W., Li, F. K., Canizares, C., et al. 1977, *MNRAS*, 179, 651. doi:10.1093/mnras/179.4.651
- Cui, W., Morgan, E. H., & Titarchuk, L. G. 1998, *ApJL*, 504, L27. doi:10.1086/311569
- Farrell, S. A., Barret, D., & Skinner, G. K. 2009, *MNRAS*, 393, 139. doi:10.1111/j.1365-2966.2008.14167.x
- García, F., Zhang, G., & Méndez, M. 2013, *MNRAS*, 429, 3266. doi:10.1093/mnras/sts583
- Giacconi, R., Murray, S., Gursky, H., et al. 1974, *ApJS*, 27, 37. doi:10.1086/190288
- Grindlay, J., Gursky, H., Schnopper, H., et al. 1976, *ApJL*, 205, L127. doi:10.1086/182105
- Grindlay, J. E. 1986, *The Evolution of Galactic X-Ray Binaries*, 167, 25
- Grindlay, J. E. 1988, *The Harlow-Shapley Symposium on Globular Cluster Systems in Galaxies*, 126, 347
- Haberl, F., Stella, L., White, N. E., et al. 1987, *ApJ*, 314, 266. doi:10.1086/165056
- Hameury, J. M., King, A. R., & Lasota, J. P. 1986, *A&A*, 162, 71
- Horne, J. H. & Baliunas, S. L. 1986, *ApJ*, 302, 757.
doi:10.1086/164037
- Jahoda, K., Swank, J. H., Giles, A. B., et al. 1996, *Proc. SPIE*, 2808, 59. doi:10.1117/12.256034
- in't Zand, J., Serino, M., Kawai, N., et al. 2011, *The Astronomer's Telegram*, 3625

- Jain, C. & Paul, B. 2011, *MNRAS*, 413, 2.
doi:10.1111/j.1365-2966.2010.18110.x
- Jain, C., Sharma, R., & Paul, B. 2022, *MNRAS*, 517, 2131.
doi:10.1093/mnras/stac2804
- Kotze, M. M. & Charles, P. A. 2012, *MNRAS*, 420, 1575.
doi:10.1111/j.1365-2966.2011.20146.x
- Levine, A. M., Bradt, H., Cui, W., et al. 1996, *ApJL*, 469, L33. doi:10.1086/310260
- Markwardt, C. B. 2006, *The Transient Milky Way: A Perspective for MIRAX*, 840, 45. doi:10.1063/1.2216601
- Matsuoka, M., Kawasaki, K., Ueno, S., et al. 2009, *PASJ*, 61, 999. doi:10.1093/pasj/61.5.999
- Mazeh, T. & Shaham, J. 1979, *A&A*, 77, 1
- Meegan, C., Lichti, G., Bhat, P. N., et al. 2009, *ApJ*, 702, 791. doi:10.1088/0004-637X/702/1/791
- Menou, K., Perna, R., & Hernquist, L. 2002, *ApJL*, 564, L81. doi:10.1086/338909
- Nasa High Energy Astrophysics Science Archive Research Center (Heasarc) 2014, *Astrophysics Source Code Library*. ascl:1408.004
- Paczyński, B. 1971, *ARA&A*, 9, 183.
doi:10.1146/annurev.aa.09.090171.001151
- Patruno, A. & Watts, A. L. 2021, *Timing Neutron Stars: Pulsations, Oscillations and Explosions*, 461, 143.
doi:10.1007/978-3-662-62110-3_4
- Peuten, M., Brockamp, M., Küpper, A. H. W., et al. 2014, *ApJ*, 795, 116. doi:10.1088/0004-637X/795/2/116
- Ponti, G., De, K., Muñoz-Darias, T., et al. 2017, *MNRAS*, 464, 840. doi:10.1093/mnras/stw2317
- Press, W. H., Teukolsky, S. A., Vetterling, W. T., et al. 2002, *Numerical recipes in C++ : the art of scientific computing by William H. Press*. xxviii, 1,002 p. : ill. ; 26 cm. Includes bibliographical references and index. ISBN : 0521750334
- Priedhorsky, W. & Terrell, J. 1984, *ApJL*, 284, L17.
doi:10.1086/184343
- Pringle, J. E. 1981, *ARA&A*, 19, 137.
doi:10.1146/annurev.aa.19.090181.001033
- Rappaport, S., Nelson, L. A., Ma, C. P., et al. 1987, *ApJ*, 322, 842. doi:10.1086/165778
- Šimon, V. 2003, *A&A*, 405, 199.
doi:10.1051/0004-6361:20030514
- Scargle, J. D. 1982, *ApJ*, 263, 835. doi:10.1086/160554
- Serino, M., Iwakiri, W., Negoro, H., et al. 2021a, *The Astronomer's Telegram*, 14871
- Serino, M., Iwakiri, W., Negoro, H., et al. 2021b, *The Astronomer's Telegram*, 15071
- Smale, A. P. & Lochner, J. C. 1992, *ApJ*, 395, 582.
doi:10.1086/171678
- Spruit, H. C. 2010, arXiv:1005.5279.
doi:10.48550/arXiv.1005.5279
- Stella, L., Kahn, S. M., & Grindlay, J. E. 1984, *ApJ*, 282, 713. doi:10.1086/162253
- Stella, L., Priedhorsky, W., & White, N. E. 1987, *ApJL*, 312, L17. doi:10.1086/184811
- Strohmayer, T. E. & Brown, E. F. 2002, *ApJ*, 566, 1045.
doi:10.1086/338337
- Tan, J., Morgan, E., Lewin, W. H. G., et al. 1991, *ApJ*, 374, 291. doi:10.1086/170118
- Tavani, M. 1991, *Nature*, 351, 39. doi:10.1038/351039a0
- Tsunemi, H., Kitamoto, S., Manabe, M., et al. 1989, *PASJ*, 41, 391
- Vacca, W. D., Lewin, W. H. G., & van Paradijs, J. 1986, *MNRAS*, 220, 339. doi:10.1093/mnras/220.2.339
- van der Klis, M., Hasinger, G., Dotani, T., et al. 1993a, *MNRAS*, 260, 686. doi:10.1093/mnras/260.3.686
- van der Klis, M., Hasinger, G., Verbunt, F., et al. 1993b, *A&A*, 279, L21
- Wang, Z. & Chakrabarty, D. 2010, *ApJ*, 712, 653.
doi:10.1088/0004-637X/712/1/653
- Wen, L., Levine, A. M., Corbet, R. H. D., et al. 2006, *ApJS*, 163, 372. doi:10.1086/500648
- Wilson-Hodge, C. A., Case, G. L., Cherry, M. L., et al. 2012, *ApJS*, 201, 33. doi:10.1088/0067-0049/201/2/33
- Wolff, M. T., Ray, P. S., Wood, K. S., et al. 2009, *ApJS*, 183, 156. doi:10.1088/0067-0049/183/1/156
- Yu, W., Li, Z., Lu, Y., et al. 2024, *A&A*, 683, A93.
doi:10.1051/0004-6361/202348195
- Yuan, W. & Osborne, J. P. 2015, arXiv:1506.07736.
doi:10.48550/arXiv.1506.07736
- Zdziarski, A. A., Wen, L., & Gierliński, M. 2007a, *MNRAS*, 377, 1006. doi:10.1111/j.1365-2966.2007.11686.x
- Zdziarski, A. A., Gierliński, M., Wen, L., et al. 2007b, *MNRAS*, 377, 1017. doi:10.1111/j.1365-2966.2007.11688.x